Characterization of hen phosvitin in aqueous salt solutions: Size, structure, and aggregation

Machi Takeuchi [a,d], Tsuyoshi Mashima [b,d], Michael Sztucki [e], Andrei V. Petukhov [a,f], Mark Vis [a,d], Heiner Friedrich [a,c,d], Remco Tuinier [a,d,*]

[a] *Laboratory of Physical Chemistry, Department of Chemical Engineering and Chemistry, Eindhoven University of Technology, P.O. Box 513, 5600 MB, Eindhoven, the Netherlands*
[b] *Laboratory of Chemical Biology, Department of Biomedical Engineering, Eindhoven University of Technology, P.O. Box 513, 5600 MB, Eindhoven, the Netherlands*
[c] *Center for Multiscale Electron Microscopy, Department of Chemical Engineering and Chemistry, Eindhoven University of Technology, Het Kranenveld 14, 5600 MB, Eindhoven, the Netherlands*
[d] *Institute for Complex Molecular Systems, Eindhoven University of Technology, P.O. Box 513, 5600 MB, Eindhoven, the Netherlands*
[e] *ESRF, The European Synchrotron, 71 Avenue des Martyrs, CS40220, 38043, Grenoble Cedex 9, France*
[f] *Van 't Hoff Laboratory for Physical and Colloid Chemistry, Debye Institute, Utrecht University, Padualaan 8, 3584 CH, Utrecht, the Netherlands*

ARTICLE INFO

ABSTRACT

Phosvitins is a key egg yolk protein and can often be found in food emulsions. It is highly phosphorylated and hence phosvitins contain a large number of negatively charged amino acid groups, for pH > pI. Due to the presence of these phophoserines, phosvitins bind to positively charged multivalent ions. Its amphipolar structure makes phosvitin also an efficient emulsion stabilizer. The ion binding and emulsifying abilities of phosvitins are influenced by environmental conditions such as pH and ionic strength. Various physicochemical properties of phosvitins such as size and charge under various conditions, and how they self-assemble via multivalent ions are not well-understood. To gain more insight into these physical characteristics, we performed high brilliance synchrotron small angle X-ray scattering (SAXS) on phosvitin solutions. The structure factor $S(q)$ obtained from the SAXS profiles showed that the double layer interactions between charged phosvitin assemblies are strongly affected by pH and ionic strength of the buffer. The effects of multivalent ions (Mg^{2+}, Fe^{3+}) on the size and structure of phosvitin were also investigated. Our results revealed that the aggregation of phosvitin mediated by metal ions is induced by electrostatic attraction and only occurs beyond a threshold cation concentration, where phosvitin loses long-range electrostatic double layer repulsions. These findings help understanding the effects of metal ions and pH on phosvitin in more complex environments such as food emulsions.

1. Introduction

Phosvitins are phosphoproteins and account for 16% of egg yolk granules and are part of a wide range of food products (Anton, 2013; Huopalahti, López-Fandiño, Anton, & Schade, 2007). They are highly phosphorylated and consist of about 200 amino acids and have a molar mass of 35–40 kDa (Byrne et al., 1984; Huopalahti et al., 2007; Taborsky, 1983). Phosvitins can be separated into α- and β-phosvitin isoforms, with different molar masses of their sub-units (Huopalahti et al., 2007). The amino acid composition of a phosvitin molecule is similar to that of a triblock copolymer: a long central hydrophilic peptide chain 'block' of about 100 phosphorylated serine residues is connected to two smaller

outer 'blocks' containing mainly hydrophobic amino acids (Huopalahti et al., 2007). Phosvitin's middle block contains a large number of negatively charged phosphoric acid groups for pH ≫ pI (Damodaran & Xu, 1996), with pI the isoelectric point. In aqueous (salt) solutions all phosphorylated groups are protonated at pH < pI and the few positively charged amino acids e.g. arginine and lysine then provide a net positive charge. It has been reported that the isoelectric point of phosvitin is just below pH ≈ 2 (Taborsky, 1968), so for most common solution conditions with pH > 2 phosvitins are (highly) negatively charged. A significant conformational change of phosvitin from a random coil to sheet-like is known to occur at pH ≈ 2 (Damodaran & Xu, 1996; Taborsky, 1968; Yasui et al., 1990). Due to the large number of charged phosphoserine

---

groups, phosvitins are ion-chelating for biologically essential multivalent ions such as magnesium, calcium and iron, and the binding capacity is strongly affected by pH or ionic strength (Griz-zuti & Perlmann, 1973, 1975; Yilmaz & Ağagündüz, 2020). This may explain the abundance of phosvitins in eggs for the hatchling.

Although the biological function of phosvitin is not fully understood yet, some findings have been reported (Onuma, 2005; Zhang, Geng, Huang, & Ma, 2016; Zhang, Huang, & Ma, 2017). Phosvitin seemed to have an effect on the nucleation and growth of hydroxyapatite (Onuma, 2005; Zhang et al., 2017), which is a main mineral constituent of human/animal bone. Zhang et al. (Zhang et al., 2016) studied thermodynamic aspects of the complexation mechanism between phosvitin and calcium ions, which might help to understand the role of phosvitin in biomineralization.

Phosvitin is often applied in food emulsions as it acts as stabilizer and it is naturally present in egg yolk-derived emulsions. In food emulsions, chelation of iron by phosvitins has been suggested to play a vital role in lipid oxidation of food emulsions (Yilmaz & Ağagündüz, 2020), and therefore the anti-oxidant activity of phosvitins by chelating such pro-oxidant metals has received interest (Duan et al., 2016; Jiang et al., 2020; Lee, Han, & Decker, 2002; Lu & Baker, 1986). Lipid oxidation is a long-standing problem since it limits the shelf-life of food products. Oxidation is caused by a free radical chain reaction promoted by the reduction-oxidation (redox) reaction of multivalent metal ions (Berton-Carabin, Ropers, & Genot, 2014). Recently, it has been found that ferric irons bound to phosvitins may be one of the main pro-oxidants in food emulsions since the ferric iron from phosvitins is considered to be released at acidic pH, leading to promote the radical reaction of the lipid phase (Merkx, Delić, Wierenga, Hennebelle, & van Duynhoven, 2019). The influence of ionic strength and pH on the iron ion binding of phosvitins has been studied by Castellani et al. (Castellani, Guérin-Dubiard, David-Briand, & Anton, 2004). Their results showed that near pH ≈ 7 the iron binding capacity of phosvitins was highest at low ionic strength. They also argued that adding salt ions to aqueous solutions screens the charge of phosvitin, which reduces the electrostatic driving force for phosvitin to bind iron ions. In contrast, an increase in iron binding capacity was observed at high ionic strength at acidic pH conditions. Under acidic conditions the driving electrostatic force is probably less significant compared to neutral pH because then most of the phosphoserine groups are protonated. Consequently, at acidic pH a decrease of the range of the double layer interactions by added salt leads to a better binding capacity of phosvitins for iron ions.

The above clarifies the important role of phosvitins as emulsifiers of oil-in-water emulsions in many egg-derived foods (Castellani, Belhomme, David-Briand, Guérin-Dubiard, & Anton, 2008; Kato, Miyazaki, Kawamoto, & Kobayashi, 1987). The surface activity of phosvitins at an oil-water interface is driven by the triblock-like structure (Fleer, Cohen Stuart, Scheutjens, Cosgrove, & Vincent, 1998) of phosvitin, with two relatively hydrophobic outer blocks and a large hydrophilic charged block. As the electrostatic interaction between charged phosphate groups has a great influence on stabilizing the emulsion droplets (Kato et al., 1987), the presence of added Mg^{2+} and Fe ions affects the emulsifying ability of phosvitins due to screening and ion complexation of the phosphoric acid groups (Castellani et al., 2008). Although phosvitins have essential roles as ion binder and emulsifier in food emulsions, the fundamental physicochemical properties of phosvitin such as size, aggregation behavior, and charge and influence of multivalent cations are not well understood yet.

The aim of this study is hence to gain more insights into the effect of pH, ionic strength, and multivalent cations on phosvitin. To study the effect of pH on the physical-chemical properties of phosvitins in aqueous solution, pH values of 2 and 7 were selected. These values are slightly beyond the common pH range in food systems, which lies between pH 3 and pH 6 (Bridges & Mattice, 1939), although even alkaline food products exist. This is also on account that the net charge of phosvitin nearly vanishes at pH 2 and it increases at higher pH. The systems in

between can be interpreted as intermediate cases. Moreover, phosvitin solutions at pH 4 and pH 7 with different salt concentrations were investigated. Here, we selected pH 4 instead of pH 2 to evaluate the effects of salt concentration at conditions relevant for food systems. The studied buffer concentrations of 5–100 mM correspond to 0.8–16 g/L and 0.3–6.5 g/L of potassium phosphate buffer and acetate buffer, respectively. This is similar to the order of magnitude of the salt concentrations found in food systems, as the salt concentration in food products varies between 0.1 and 4.0 g per 100 g (Angus, 2007). The influence of Mg^{2+} and Fe^{3+} were especially studied as biologically and nutritionally relevant cations. Small angle X-ray scattering (SAXS) with high brilliance synchrotron radiation was employed as it can be used to characterize the structure of complex biomolecules and their interactions in solution, which usually have low concentration and weak scattering of samples (Jeffries et al., 2021; Skou, Gillilan, & Ando, 2014; Svergun & Koch, 2003). Double layer interactions between charged phosvitins were confirmed from the structure factor $S(q)$, including how it was affected by pH and ionic strength of the buffer. We also studied how phosvitin assembled with multivalent ions.

2. Materials and methods

2.1. Materials

Fresh hen eggs were obtained from a local supermarket. Eggs were used within 24 h of purchase. Meanwhile, the eggs were stored in a fridge (4 °C). They were used at least two weeks before the expiration date. Potassium phosphate monobasic (≥99.0%), potassium phosphate dibasic (98.0–100.5%), sodium acetate trihydrate (≥99.5%), sodium hydroxide (NaOH, ≥98%), 1,4-dithiothreitol (DTT, ≥99.0%), and $Fe(NH_4)_2(SO_4)_2 \cdot 6H_2O$ (≥99.0%) were all purchased from Sigma-Aldrich (Merck). Acetic acid was obtained from Fisher Chemical™. Hydrochloric acid (37%) was from VWR chemicals. 1 M $MgCl_2$ was purchased from Invitrogen™ Thermo Fisher Scientific (Molecular Biology Grade).

2.2. Purification of phosvitin

Purification of phosvitin was performed with anion exchange chromatography (AEC) following a previously published (Zhang, Qiu, Geng, & Ma, 2011) purification protocol. Zhang et al. (Zhang et al., 2011) employed ethylenediaminetetraacetic acid disodium salt (Na_2EDTA) during AEC to obtain metal-free phosvitin. We did not use Na_2EDTA during purification of phosvitin to study the protein in its native state as used in food emulsions. Besides the above purification, size exclusion chromatography (SEC) (Bio-Rad NGC chromatography system with GE healthcare HiLoad Superdex 200 16/600, eluent: 100 mM potassium phosphate buffer, pH 7) was performed to further purify phosvitin. Analytical SEC was performed to estimate the molar mass of purified phosvitin (see the Supporting Information, section S1). Sodium dodecyl sulphate–polyacrylamide gel electrophoresis (SDS-PAGE) was conducted to evaluate the purity of the obtained phosvitin. Samples were heated at 95 °C for 5 min in sample buffer (Laemmli Sample Buffer (Bio-Rad) and 50 mM DTT) and run on pre-cast 4–20% Mini-PROTEAN® TGX gels (Bio-Rad) in running buffer (Tris/Glycine/SDS Buffer, Bio-Rad) for 35 min at 180 V. Precision Plus Protein™ All Blue Standards (Bio-Rad) was used as a reference. Gels were stained with Coomassie Brilliant Blue G-250 (Bio-Rad). An image of the gel was acquired using an ImageQuant 400 Digital Imager (GE Healthcare). The purified phosvitin solution was rapidly frozen by liquid nitrogen and stored at a temperature $T = -20$ °C prior to further use.

2.3. Sample preparation

The phosvitin concentration was determined by absorption at a wavelength $\lambda = 280$ nm (Castellani, Martinet, David-Briand,

Guérin-Dubiard, & Anton, 2003). Dialysis was conducted to exchange 100 mM potassium phosphate buffer (pH 7) with the desired buffer and pH (MWCO 10 kDa, Slide-A-Lyzer™ MINI Dialysis Unit, Thermo Scientific™). Monopotassium phosphate was used for preparing a phosvitin solution at pH 2, and acetate buffer was used for a phosvitin solution at pH 4. The pH of these buffers was adjusted either by 6 M HCl or 6 M NaOH. The final pH after dialysis was measured by using pH-indicator strips. The range of salt concentrations C of the salts (MgCl$_2$ and Fe(NH$_4$)$_2$(SO$_4$)$_2$) studied was estimated based on the total amount of ion binding sites available in the phosvitin molecule (Castellani et al., 2004) (for details see section 3.3). Also, from dynamic light scattering (DLS) the appropriate salt concentration regime was verified by checking variations in size (see the Supporting Information, section S2). To study the effect of metal ions on phosvitin assembly, a stock solution of phosvitin (10 mM potassium phosphate buffer, pH 7) was mixed with an aqueous stock solution of 100 mM MgCl$_2$ or a 10 mM Fe(NH$_4$)$_2$(SO$_4$)$_2$ in 10 mM HCl solution (Castellani et al., 2004) to arrive at the target concentrations of the protein and salt. Each dispersion was mixed for 30 min with MixMate® (Eppendorf). Oxidation of ferrous irons into ferric irons occurs upon binding with phosvitin (Taborsky, 1963). These samples were stored at $T = -20$ °C, and defrosted before the SAXS measurement.

2.4. Small angle X-ray scattering (SAXS)

The SAXS measurements on phosvitin solutions were performed at the ID02 beamline of the European Synchrotron Radiation Facility (ESRF) in Grenoble, France (Narayanan et al., 2018, 2022). Table 1 summarizes the experimental conditions of the SAXS measurements.

2.5. Data analysis

The normalized scattering intensity $I(q)$ of SAXS is described using Rayleigh-Gans-Debye theory and can be written as (Jeffries et al., 2021; Ottewill, 1997a, 1997b):

$$I(q) \approx NV^2(\Delta\rho)^2 P(q)S(q). \tag{1}$$

N is the particle concentration (number per unit) volume and V is the volume of the particle that scatters. In our study, the particle is considered as α-phosvitin, which consists of 3–4 phosvitin molecules (see section 3.1). The quantity $\Delta\rho$ is the scattering length density difference between the particle and the medium; it quantifies the scattering contrast. In our system $\Delta\rho$ is defined by $\Delta\rho = \rho_{\text{phosvitin}} - \rho_{\text{buffer}}$. The form factor $P(q)$ quantifies the interference between scattered waves from different points within the same particle, so it reflects the intraparticle structure. The structure factor $S(q)$ represents the interference between scattered waves from different particles and hence accounts for the average interparticle distance of the system, which depends on the interactions between the particles. It should be noted that the factorization of the scattering intensity into the form- and structure-factors is strictly correct only for monodisperse spherical particles. In other cases it can be considered an approximation (Dhont, 1996). This factorization provides useful semi-quantitative insights because it enables to separate intra-

and inter-particle structure of the dispersion and is often applied. Both $P(q)$ and $S(q)$ are a function of the scattering wave vector q, which is defined as:

$$q = \frac{4\pi}{\lambda_{\text{m}}}\sin\left(\frac{\theta}{2}\right), \tag{2}$$

where λ_{m} is the radiation wavelength in the medium and θ is the scattering angle. One can estimate the typical length scale Λ that is probed at a certain value of q using:

$$\Lambda = \frac{2\pi}{q}. \tag{3}$$

In case of hard spheres the first (low q) maximum of $S(q)$ corresponds to $\Lambda = d$, with d the diameter of the hard spheres (de Kruif, Briels, Vrij, & May 1988).

To estimate the radius of gyration R_g of the structures from the SAXS profile from dilute samples, the Guinier approximation was employed (Ottewill, 1997b):

$$I(q) = I(0)\exp\left(-\frac{q^2 R_g^2}{3}\right). \tag{4}$$

The range for which the Guinier approximation is accurate is $qR_g \lesssim 1.3$ (Guinier & Fournet, 1955). In the limit q approaching zero the scattered intensity $I(0)$ can be determined.

Experimentally, we have found that a 1 mg/mL phosvitin solution appeared to be sufficiently dilute to assume $S(q) = 1$. Beyond dilute particle concentrations, $S(q)$ deviates from unity. In that case $S(q)$ can be determined experimentally by:

$$S(q) = \frac{I(q)}{I_{\text{dil}}(q)}\frac{C_{\text{dil}}}{C}, \tag{5}$$

where $I_{\text{dil}}(q)$ and C_{dil} are the scattered intensity and the concentration of a dilute system for which $S(q)$ approaching one. The structure factor at q approaching zero can be related to the second virial coefficient (B_2) through the osmotic compressibility:

$$S(q \to 0) = \frac{\partial\varphi}{\partial\widetilde{\Pi}} \approx \exp\left(-\frac{2B_2}{V}\varphi\right), \tag{6}$$

where $\widetilde{\Pi}$ is the normalized osmotic pressure ($= \Pi V/kT$), φ is the particle volume fraction, and V is the particle volume.

Background subtraction of the acquired SAXS data was performed with the SAXS data of 10 mM potassium phosphate buffer solution or that of demineralized water.

3. Results and discussion

3.1. Purification of phosvitin

To obtain high-purity phosvitin for the scattering studies, size exclusion chromatography (SEC) was performed to remove impurities from phosvitin solutions after isolating phosvitin from egg with anion-exchange chromatography. The SEC trace showed a clear peak at the elution volume of 66–86 mL (Fig. 1A). Purity of the eluted fraction was analyzed by SDS-PAGE (Fig. 1B). The band corresponding to about 35 kDa is considered to correspond to individual phosvitin molecules (Huopalahti et al., 2007). In contrast, the eluted solution without SEC had multiple bands in the SDS-PAGE electrophoretogram, which were remaining impurities from egg yolk. We used the high-purity phosvitin obtained from elution fraction I in the SEC trace to prepare dispersions for the scattering measurements. To evaluate the molar mass (M) of the obtained phosvitin, analytical SEC was conducted (for details see the Supporting Information, section S1). The trace of analytical SEC revealed that the molar mass M of the purified phosvitin after SEC was
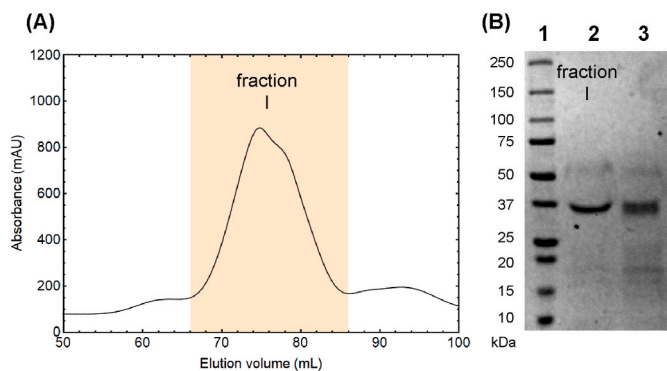
Table 1
Experimental conditions of the SAXS measurements at beamline ID02 at the ESRF.

	Measurement parameters
Operating energy (keV)	12.4
Wavelength (nm)	0.1
Detector distance (m)	3.0
q range (Å^{-1})	0.002–0.25
Temperature (°C)	Room temperature
Detector	Eiger2X 4M
Sample holder	Flow-through capillary (⌀ = 1.9 mm)

Fig. 1. (**A**) Size exclusion chromatography (SEC) trace of the phosvitin sample after anion exchange chromatography (AEC). 100 mM potassium phosphate buffer at pH 7 was used as an eluent. Absorbance was measured at a wavelength of $\lambda = 230$ nm. Eluted fraction I was collected and used for further light and X-ray scattering experiment. (**B**) SDS-PAGE electrophoretogram of the purified phosvitin. Lane 1: precision Plus Protein™ All Blue Standards (Bio-Rad), lane 2: eluted fraction I of phosvitin solution after SEC, lane 3: phosvitin solution after AEC. (For interpretation of the references to colour in this figure legend, the reader is referred to the Web version of this article.)

about 140 kDa. Therefore, the purified phosvitin is expected to be α-phosvitin composed of 3–4 individual phosvitin subunits of 35 kDa (Huopalahti et al., 2007).

3.2. The effect of pH and ionic strength on the interactions between phosvitins

The size and interaction between α-phosvitins at pH 2 and pH 7 were evaluated by SAXS. Hereafter, phosvitin refers to α-phosvitin. The wave vector dependence of the scattered intensities are plotted in Fig. 2A and C.

Distinct SAXS scattering profiles of phosvitin solutions for various phosvitin concentrations were studied at the two pH values. At pH 7, a broad scattering peak appears which shifts to larger q with increasing phosvitin concentration (Fig. 2A). This peak and its concentration dependence can be related to repulsive electrostatic interactions between proteins (Zhang et al., 2007).

At pH 7 all the phosphoserine residues in phosvitin molecules are considered to be negatively charged (for details see the Supporting Information, section S3 Fig. S5) and upon increasing the protein concentration the effective Debye length decreases (Heinen, Holmqvist, Banchio, & Nägele, 2011; Van Gruijthuijsen, Obiols-Rabasa, Heinen, Nägele, & Stradner, 2013) as charged proteins act as macro-ions, which contribute to electrostatic screening.

To quantify the structure of the dispersion, which depends on the interactions between phosvitins and their concentration, the structure factor $S(q)$ was obtained from the scattering profile using equation (5)
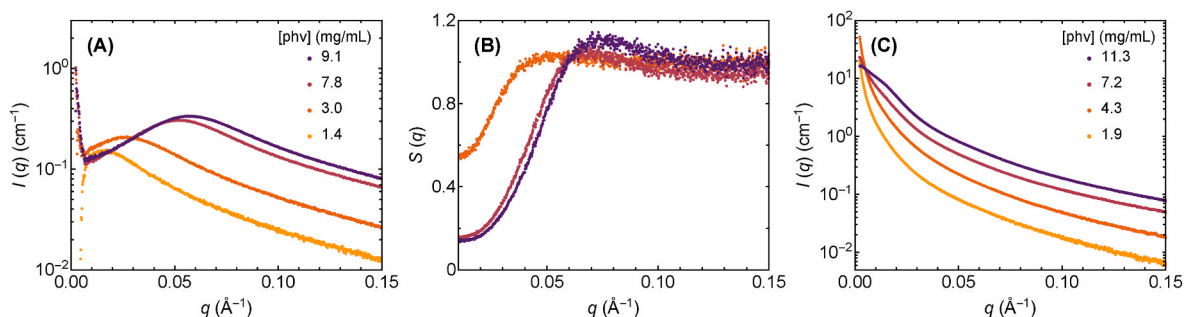
(Fig. 2B). The scattering profile from the most dilute system with concentration C_{dil} was used as I_{dil}. In Fig. 2B, maxima in $S(q)$ appear around $q \approx 0.08$ Å^{-1} for phosvitin concentrations of 7.8 and 9.1 mg/mL, while for 3.0 mg/mL the maximum is close to $q \approx 0.045$ Å^{-1}. The concentration dependence of $S(q)$ appears similar as for suspensions of charged colloidal spheres, such as charged silica particles dispersions (Philipse & Vrij, 1988), where a peak shift and peak maxima were observed with an increase in the volume fraction of the particle. From the position of the peaks, the typical interparticle (center-to-center) distance d_{eff} of phosvitins was estimated from equation (3) to be about $d_{eff} = 8$ nm for 7.8 & 9.1 mg/mL and $d_{eff} \approx 14$ nm for 3.0 mg/mL. We infer that the phosvitin particles in the solution can get closer to each other at higher concentration due to a decrease in the Debye screening length.

The effective interaction radius of phosvitin $r_{eff} = d_{eff}/2$ was studied by employing equation (6) and was compared with the radius of gyration R_g. For uncharged particles $R_g = r_{eff}(3/5)^{1/2}$ is expected (de Kruif et al., 1988). Like-charged colloidal spheres repel each other, resulting in $r_{eff} \gg R_g$. In equation (6), the normalized second virial coefficient ($B_2^* = B_2/V$) was assumed as $B_2^* = 4$ for hard spheres. From Fig. 2B, $S(q \to 0)$ was considered to be $S(q \to 0) \approx 0.55$ for $C = 3.0$ mg/mL and subsequently an effective volume fraction $\varphi_{eff} \approx 0.075$ was obtained. The theoretical volume fraction in the system φ of phosvitin is $\varphi \approx 0.004$. This was calculated by taking the radius of gyration ($R_g = 4.1$ nm), which is obtained by the Guinier approximation of phosvitin solution in 10 mM potassium phosphate buffer (see section 3.3), as protein radius. The ratio of volume fractions $(\varphi_{eff}/\varphi)^{1/3}$ gives $r_{eff} \approx 11$ nm for phosvitin, assuming that phosvitins are spherical. The large r_{eff} compared to R_g suggests that phosvitins at pH 7 behave as colloidal particles that interact through a significant long-ranged double layer repulsion, originating from the presence of the negatively charged phosphoserines. This implies that the effective volume and interactions of phosvitin in aqueous solution are sensitive to salt concentration and the type of salts at this pH.

The scattering intensity profiles of phosvitin at pH 2, see Fig. 2C, differ substantially from the SAXS data at pH 7 in Fig. 2A. At pH = 2 phosvitins are close to their isoelectric point, so the electrostatic interactions are weak. In case of pH ≤ 2, most phosphorylated groups become protonated. Furthermore, the different secondary structure of phosvitin between pH 2 and pH 7 might also play a role in the differences between the SAXS profiles. By increasing the phosvitin concentration from 1.9 mg/mL to 11.3 mg/mL, an increase in scattered intensity was observed and the overall intensity was much higher than the one at pH 7. A tiny peak, emerging at $q \approx 0.015$ Å^{-1} could imply a weak electrostatic repulsive force. This is possibly because of slightly charged phosphoserine groups from phosvitins at pH 2.

The salt concentration also has an influence on the pair interaction of phosvitins. Fig. 3 shows the scattered SAXS intensity of phosvitin solution at pH 7 (Fig. 3A) and pH 4 (Fig. 3B) for different buffer concentrations. The phosvitin concentration was kept constant at 1.3 mg/mL for pH 4 and 1.4 mg/mL for pH 7. The difference in the protein
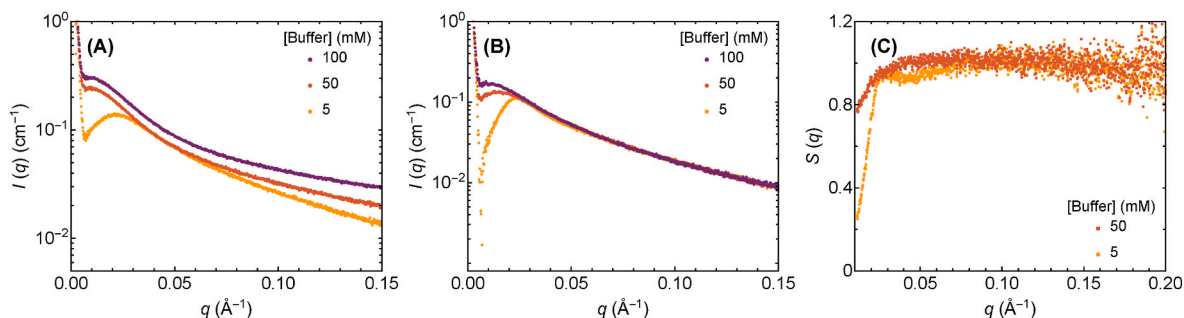

Fig. 2. SAXS data measured at different phosvitin (phv) concentrations. (**A**) Scattering profiles of phosvitin solutions at pH 7. (**B**) Structure factor $S(q)$ at pH 7 derived using equation (5) from the data in the panel (**A**). (**C**) Scattering profiles of phosvitin solutions at pH 2.

Fig. 3. SAXS data measured at different buffer concentrations. Scattering profiles of phosvitin solutions at pH 7 (**A**) and at pH 4 (**B**). Panel (**C**) shows structure factor $S(q)$ at pH 4 derived from the data in the panel (**B**) by applying equation (5).

concentration between these pH values does not influence the obtained results as the scattered intensity profile from SAXS profile is hardly affected within this concentration regime (see Fig. 2). At pH 4 phosvitins still contain a significant number of negatively charged groups, as pH > pI ≈ 2. At both pH 4 and pH 7, the downturn at $q \approx 0.02$ Å^{-1} for 5 mM buffer concentration gradually disappeared with increasing in buffer concentration. The structure factor $S(q)$ for the phosvitin solution at pH 4 was also determined by using equation (5) (Fig. 3C). It is important to note that in this case the scattering profile of 100 mM buffer concentration (C_{dil}) was used as I_{dil} as it reflects a condition where $S(q) \approx 1$ is attained. Fig. 3C shows $S(q \to 0) \approx 0.25$ and $S(q \to 0) \approx 0.77$ for buffer concentration of 5 mM and 50 mM, respectively. By using equation (6) effective volume fractions φ_{eff} were calculated to be $\varphi_{eff} \approx 0.17$ for 5 mM buffer and $\varphi_{eff} \approx 0.03$ for 50 mM buffer. This expectedly points to a decrease in the Debye screening length by increasing the salt concentration. For pH 7, it was not possible to properly analyze the structure factor due to the change at high q range in scattered intensity profile upon increasing buffer concentration. This is related with a change in the form factor $P(q)$ of phosvitin. It could be that the phosphate buffer has an influence on the intramolecular interactions of phosphoric acid groups of phosvitin, resulting in the different $P(q)$ by increasing buffer concentration. However, from the forward scattered intensity $I(q \to 0)$ in Fig. 3A an increased scattered intensity as well as a peak shift towards low q was detected with increasing buffer concentration. This can infer that the effective volume of phosvitin φ_{eff} is decreased by increasing buffer salt concentration, leading to a decrease in the effective volume of the protein.

3.3. Ion-induced assembly of phosvitin

The effect of multivalent ions such as Mg^{2+} and Fe^{3+} ions on the size and structure of phosvitin at pH 7 was characterized by SAXS. In Fig. 4A, the scattering intensity $I(q)$ was plotted as a function of wave vector q for different $MgCl_2$ concentrations ($C_{Mg^{2+}}$). For $C_{Mg^{2+}} \leq 6$ mM, mainly an

increase of the overall scattering intensity was observed upon increasing $C_{Mg^{2+}}$. As a change in the shape of the scattering curves at $C_{Mg^{2+}} \leq 6$ mM was nearly imperceptible, the increased intensity is attributed to an increase in the scattering contrast $\Delta\rho$ due to the presence of Mg^{2+} ions that complex with phosvitin. When Mg^{2+} ions adsorb onto phosvitin, the mass increases about 5% and we believe that this is responsible for the large increase in the scattering contrast. The scattering length density of the solvent does not change significantly at these low Mg^{2+} concentrations. For $C_{Mg^{2+}} = 8$ mM, the scattering curve looks very different, implying that different structures formed in the dilute phosvitin solution. For the studied phosvitin concentration (1.5 mg/mL), the available concentration of ion binding sites in α-phosvitin is calculated to be about 2.6 mM, by assuming that one phosvitin molecule (35 kDa) has 123 phosphoserines where two phosphoric acid groups bind 1 Mg^{2+} ion (Castellani et al., 2004). 3-fold excess of Mg^{2+} until aggregation of phosvitin is observed.

We applied the Guinier approximation (see equation (4)) in the q range of 0.01 Å$^{-1} \leq q \leq 0.02$ Å^{-1} for the SAXS intensity profile of 8 mM $MgCl_2$ concentration and 0.02 Å$^{-1} \leq q \leq 0.03$ Å^{-1} for the rest of the SAXS profiles to analyze the radius of gyration R_g of the phosvitin complexes with Mg^{2+} ions. We assumed that the structure factor $S(q) \to 1$, as the phosvitin concentration was low (1.5 mg/mL). From the slope of $\ln I(q)$ versus q^2 in Fig. 4B, R_g was obtained (Fig. 4C). The R_g of phosvitin before adding Mg^{2+} ions was $R_g = 4.1$ nm, and it was hardly affected up to 6 mM $MgCl_2$. For 8 mM of $MgCl_2$, R_g significantly increased to $R_g = 6.7$ nm. This suggests that phosvitin starts to form aggregates of complexes with Mg^{2+} ions (phosvitin-Mg), resulting in larger clusters about 4 times as large as the original volume. At low Mg^{2+} concentrations they complex with phosphorous groups of the phosvitins, but as the phosvitins get decorated they start to aggregate with each other to form larger clusters.

The aggregation behavior of phosvitin was also characterized by dynamic light scattering (DLS) (see the Supporting Information, section S2) by measuring intensity-averaged hydrodynamic diameter d_H for
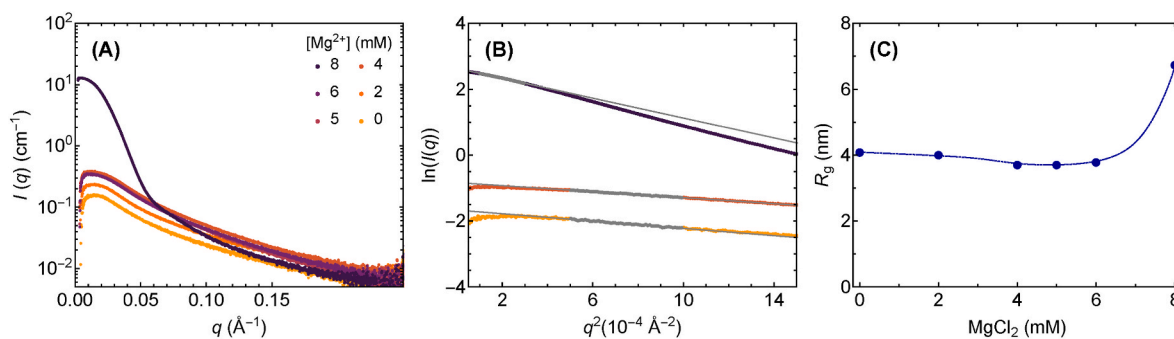

Fig. 4. (**A**) Wave vector (q) dependence of scattering intensity $I(q)$ of phosvitin solutions (1.5 mg/mL) in 10 mM potassium phosphate buffer for various Mg^{2+} concentrations. (**B**) Representative examples of fits using the Guinier approximation of the SAXS scattering profiles (0, 4, 8 mM of $MgCl_2$). Gray dots show the fitted regions and gray lines show the fits. (**C**) Radius of gyration (R_g) of phosvitin as a function of the $MgCl_2$ concentration, as obtained from the Guinier approximation.

various MgCl$_2$ concentrations. Phosvitins slowly assembled at a MgCl$_2$ concentration of 6 mM and 7 mM. At 8 mM of MgCl$_2$, there were bigger particles with $d_H \approx 25$ nm (see the Supporting Information, section S2 Fig. S2). For the DLS measurements, a small amount of 100 mM MgCl$_2$ stock solution was manually titrated to the phosvitin solution and the aggregate sizes were measured after mixing. The DLS and SAXS data revealed that phosvitin showed consistent aggregation behavior mediated by Mg^{2+} ions. We did not observe aggregation when NaCl was added to the phosvitin solution (see the Supporting Information, section S4.1 Fig. S6), which indicates the aggregation is only induced by multivalent cations as they can bridge between negatively charged phosphoserine groups.

Due to strong affinity of Fe^{3+} ions to phosvitins, the complexation of iron ions with phosvitins occurred at a much lower concentration of Fe salts (see the Supporting Information, section S4.2 Fig. S7). In the supporting Fig. S7, it was confirmed that there already is significant strong scattering in the mixture of 0.2 mM of Fe(NH$_4$)$_2$(SO$_4$)$_2$ without proteins in 10 mM potassium phosphate buffer. This is due to the formation of insoluble iron phosphate nanocomplexes in the solution. Therefore, the SAXS profiles of phosvitin solutions with Fe ions were also affected by this, especially at the lower q range of $q \leq 0.02$ Å^{-1}. However, it is still clear that the scattering of phosvitin complexes is greatly enhanced at a Fe ion concentration of 0.2 mM at $q > 0.02$ Å^{-1}, which indicates Fe^{3+} ions caused also aggregation of phosvitins.

DLS measurement of phosvitin solutions (10 mM Tris-HCl buffer, pH 7) in presence of Ca^{2+} and Fe ions was performed to further study the complexation mechanism of phosvitin with multivalent ions (the Supporting Information, section S2 Fig. S3 & Fig. S4). Upon increasing the salt concentrations, rapid increase in d_H of phosvitins was observed at $C_{Ca^{2+}} \approx 13$ mM and $C_{Fe} \approx 0.6$ mM, which implies aggregation of phosvitins. Assembly of phosvitins with Fe ions happened at lower C_{Fe} as with the SAXS data.

We hypothesize that the difference in the trend of the d_H of phosvitin as a function of the concentration of Mg^{2+} and Ca^{2+} ions might be related with the Hofmeister series, which classifies ions in accordance with their effects for physicochemical properties of proteins (Okur et al., 2017; Zhang & Cremer, 2006). Mg^{2+} ions seem to form a metastable structure with phosvitins ($d_H \approx 25$ nm) at around $C_{Mg^{2+}} \approx 8$ mM, while the d_H of phosvitin kept increasing for $C_{Ca^{2+}} \geq 13$ mM. This is in line with the Hofmeister series for cations on protein stabilization.

From above findings we propose the following phosvitin assembly model under the influence of multivalent ions. At neutral pH phosvitins are negatively charged due to many phosphoserine residues and they strongly repel each other (Fig. 5I). When multivalent cations are added into the solution, the net charge of the particles decreases and the long-range electrostatic repulsion between phosvitins decreases (Fig. 5II). Adding more multivalent cations causes aggregation of phosvitins and they form larger aggregates (Fig. 5III) as cations can anchor multiple phosvitins. The aggregation is also possibly induced by van der Waals attractions because the charge of phosvitins is considered to be sufficiently screened. For future work it is interesting to study also the zeta potential of pure phosvitin solutions to further explore the suggested mechanism of phosvitin assembly.

The studied phosvitin behavior in aqueous solutions influences their adsorption at the oil–water interface. Therefore, our investigations are relevant to the interfacial structure of emulsions stabilized by phosvitins, such as interfacial layer thickness and heterogeneity under various conditions. At neutral pH, phosvitins are highly charged and interact through an increased effective size. Thus phosvitins at the droplet interface are expected to form less dense structures, while more homogeneous and compact structures are expected at lower pH values. Low pH values or high salt concentrations can lead to aggregation of phosvitins in the aqueous phase or at the interface due to a decrease of the electrostatic double layer thickness. This might explain the observed flocculation and/or coalescence of phosvitin-containing emulsions under such conditions (Aluko & Mine, 1997; Castellani, David-Briand, Guérin-Dubiard, & Anton, 2005; Chung & Ferrier, 1992).

Probably, the interfacial structure also affects the oxidative stability of food emulsions. The interfacial region can act as a physical barrier to pro-oxidants present in the aqueous phase, which ultimately slows down lipid oxidation in the oil phase (Berton-Carabin, Sagis, & Schroën, 2018). The latter has been associated with low nutritional and sensory quality. Therefore, the insights gained on the structure of a dispersion of phosvitins and the interactions between them mediated by salt (type and concentration) and pH may help to understand how phosvitins mediate oxidation in food emulsions.

4. Concluding remarks

We have studied the physicochemical properties of phosvitin in aqueous solution such as size, charge, and electrostatic interactions. High-purity phosvitin samples were successfully prepared with an improved purification method using size-exclusion chromatography. The purified phosvitin was found to be composed of 3–4 phosvitin molecules having a molar mass of about 35 kDa.

Due to phosvitin's molecular build up containing many phosphoserine groups, pH strongly affects the size and interaction of phosvitins, which were quantitatively analyzed by determining the structure factor $S(q)$ from the obtained SAXS profiles. Most notably, it was found that the effective interaction radius of phosvitin was significantly larger than its radius of gyration at pH = 7: the structure of the phosvitin solutions is similar to that of a dispersion of charged colloidal spheres.

Furthermore, the size of phosvitin with Mg^{2+} ions was determined using small-angle X-ray scattering (SAXS) and dynamic light scattering (DLS). It was found that Mg^{2+} ions adsorb onto phosvitin at pH = 7. There appears to be a threshold cation concentration to induce assembly behavior of phosvitin. Above a concentration of about 6 mM of MgCl$_2$, which is an excess relative to the number of ion binding sites in phosvitin, an increase in the size of phosvitin was observed with both SAXS and DLS. In contrast, assembly of phosvitins with Fe^{3+} seemed to occur at much lower Fe salt concentration, even below the ion binding capacity of phosvitin. It seems that multivalent cations first complex with
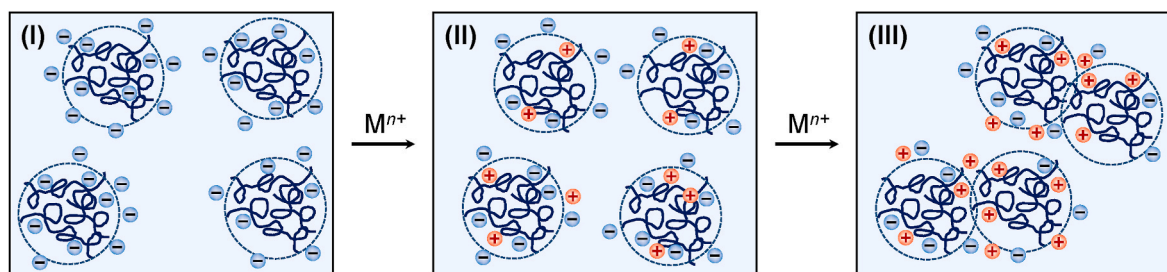

Fig. 5. Schematic of phosvitin assembly under the influence of adding multivalent ions. (**I**) Phosvitins repel each other at neutral pH. (**II**) The net charge of phosvitins decreases by adding cations. (**III**) Aggregation of phosvitins occurs once long-range electrostatic interactions are screened due to further increase of the number of complexed cations.

phosvitin via electrostatic attraction between the cations and phosphorous groups. Upon approaching full coverage, the net charge of the phosvitins vanishes and phosvitin aggregation is induced subsequently. These insights are an important basis towards understanding the influence of various conditions on the structure and adsorption behavior of phosvitins in more complex systems such as food emulsions (Berton-Carabin et al., 2018; Zhu et al., 2019).

Author statements

Machi Takeuchi, Conceptualization, Validation, Formal analysis, Investigation, Writing – Original Draft, Visualization. **Tsuyoshi Mashima**, Methodology, Investigation. **Michael Sztucki**, Methodology, Investigation. **Andrei V. Petukhov**, Writing – Review & Editing, **Mark Vis**, Formal analysis, Investigation, Writing – Review & Editing, **Heiner Friedrich**, Funding Acquisition, Writing – Review & Editing, Supervision, **Remco Tuinier**, Conceptualization, Investigation, Writing – Review & Editing, Supervision.

Declaration of competing interest

There are no conflicts of interest to declare.

Acknowledgments

Appendix A. Supplementary data

Supplementary data to this article can be found online at https://doi.org/10.1016/j.foodhyd.2022.107545.

References

Aluko, R. E., & Mine, Y. (1997). Competitive adsorption of hen's egg yolk granule lipoproteins and phosvitin in oil-in-water emulsions. *Journal of Agricultural and Food Chemistry, 45*(12), 4564–4570. https://doi.org/10.1021/jf9705328

Angus, F. (2007). *Dietary salt intake: Sources and targets for reduction.* Woodhead Publishing Limited. https://doi.org/10.1533/9781845693046.1.3

Anton, M. (2013). Egg yolk: Structures, functionalities and processes. *Journal of the Science of Food and Agriculture, 93*(12), 2871–2880. https://doi.org/10.1002/jsfa.6247

Berton-Carabin, C. C., Ropers, M. H., & Genot, C. (2014). Lipid oxidation in oil-in-water emulsions: Involvement of the interfacial layer. *Comprehensive Reviews in Food Science and Food Safety, 13*(5), 945–977. https://doi.org/10.1111/1541-4337.12097

Berton-Carabin, C. C., Sagis, L., & Schroën, K. (2018). Formation, structure, and functionality of interfacial layers in food emulsions. *Annual Review of Food Science and Technology, 9*(1), 551–587. https://doi.org/10.1146/annurev-food-030117-012405

Bridges, M. A., & Mattice, M. R. (1939). Over two thousand estimations of the pH of representative foods. *American Journal of Digestive Diseases, 6*, 440–449. https://doi.org/10.1007/BF02996505

Byrne, B. M., van het Schip, A. D., Van deKlundert, J. A., Arnberg, A. C., Gruber, M., & Ab, G. (1984). Amino acid sequence of phosvitin derived from the nucleotide sequence of part of the chicken Vitellogenin gene. *Biochemistry, 23*(19), 4275–4279. https://doi.org/10.1021/bi00314a003

Castellani, O., Belhomme, C., David-Briand, E., Guérin-Dubiard, C., & Anton, M. (2008). The role of metal ions in emulsion characteristics and flocculation behaviour of phosvitin-stabilised emulsions. *Food Hydrocolloids, 22*(7), 1243–1253. https://doi.org/10.1016/j.foodhyd.2007.08.005

Castellani, O., David-Briand, E., Guérin-Dubiard, C., & Anton, M. (2005). Effect of aggregation and sodium salt on emulsifying properties of egg yolk phosvitin. *Food Hydrocolloids, 19*(4), 769–776. https://doi.org/10.1016/j.foodhyd.2004.09.010

Castellani, O., Guérin-Dubiard, C., David-Briand, E., & Anton, M. (2004). Influence of physicochemical conditions and technological treatments on the iron binding capacity of egg yolk phosvitin. *Food Chemistry, 85*(4), 569–577. https://doi.org/10.1016/j.foodchem.2003.08.002

Castellani, O., Martinet, V., David-Briand, E., Guérin-Dubiard, C., & Anton, M. (2003). Egg yolk phosvitin: Preparation of metal-free purified protein by fast protein liquid chromatography using aqueous solvents. *Journal of Chromatography B: Analytical Technologies in the Biomedical and Life Sciences, 791*(1–2), 273–284. https://doi.org/10.1016/S1570-0232(03)00230-7

Chung, S. L., & Ferrier, L. K. (1992). pH and sodium chloride effects on emulsifying properties of egg yolk phosvitin. *Journal of Food Science, 57*(1), 40–42. https://doi.org/10.1111/j.1365-2621.1992.tb05419.x

Damodaran, S., & Xu, S. (1996). The role of electrostatic forces in anomalous adsorption behavior of phosvitin at the air/water interface. *Journal of Colloid and Interface Science, 178*(2), 426–435. https://doi.org/10.1006/jcis.1996.0137

Dhont, J. K. G. (1996). *An introduction to dynamics of colloids* (1st). Amsterdam: Elsevier.

Duan, X., Li, M., Ma, H., Xu, X., Jin, Z., & Liu, X. (2016). Physicochemical properties and antioxidant potential of phosvitin–resveratrol complexes in emulsion system. *Food Chemistry, 206*, 102–109. https://doi.org/10.1016/j.foodchem.2016.03.055

Fleer, G. J., Cohen Stuart, M. A., Scheutjens, J. M. H. M., Cosgrove, T., & Vincent, B. (1998). *Polymers at interfaces* (1st). Springer, Dordrecht. https://doi.org/10.1007/978-94-011-2130-9

Grizzuti, K., & Perlmann, G. E. (1973). Binding of magnesium and calcium ions to the phosphoglycoprotein phosvitin. *Biochemistry, 12*(22), 4399–4403. https://doi.org/10.1021/bi00746a016

Grizzuti, K., & Perlmann, G. E. (1975). Further studies on the binding of divalent cations to the phosphoglycoprotein phosvitin. *Biochemistry, 14*(10), 2171. https://doi.org/10.1016/s0021-9258(19)41063-6

Guinier, A., & Fournet, G. (1955). *Small angle scattering of X-rays.* New York: Wiley. https://doi.org/10.1002/pol.1956.120199326

Heinen, M., Holmqvist, P., Banchio, A. J., & Nägele, G. (2011). Pair structure of the hard-sphere Yukawa fluid: An improved analytic method versus simulations, Rogers-Young scheme, and experiment. *The Journal of Chemical Physics, 134*(4). https://doi.org/10.1063/1.3524309

Huopalahti, R., López-Fandiño, R., Anton, M., & Schade, R. (2007). *Bioactive egg compounds* (1st ed.). Springer-Verlag Berlin Heidelberg. https://doi.org/10.1007/978-3-540-37885-3

Jeffries, C. M., Ilavsky, J., Martel, A., Hinrichs, S., Meyer, A., Pedersen, J. S., et al. (2021). Small-angle X-ray and neutron scattering. *Nature Reviews Methods Primers, 1*(1), 70. https://doi.org/10.1038/s43586-021-00064-9

Jiang, B., Wang, X., Wang, L., Wu, S., Li, D., Liu, C., et al. (2020). Fabrication and characterization of a microemulsion stabilized by integrated phosvitin and gallic acid. *Journal of Agricultural and Food Chemistry, 68*(19), 5437–5447. https://doi.org/10.1021/acs.jafc.0c00945

Kato, A., Miyazaki, S., Kawamoto, A., & Kobayashi, K. (1987). Effects of phosphate residues on the excellent emulsifying properties of phosphoglycoprotein phosvitin. *Agricultural & Biological Chemistry, 51*(11), 2989–2994. https://doi.org/10.1080/00021369.1987.10868518

de Kruif, C. G., Briels, W. J., Vrij, A., & May, R. P. (1988). Hard-Sphere colloidal silica dispersions. The structure factor determined with SANS. *Langmuir, 4*(3), 668–676. https://doi.org/10.1021/la00081a029

Lee, S. K., Han, J. H., & Decker, E. A. (2002). Antioxidant activity of phosvitin in phosphatidylcholine liposomes and meat model systems. *Journal of Food Science, 67*(1), 37–41. https://doi.org/10.1111/j.1365-2621.2002.tb11355.x

Lu, C. L., & Baker, R. C. (1986). Characteristics of egg yolk phosvitin as an antioxidant for inhibiting metal-catalyzed phospholipid oxidations. *Poultry Science, 65*(11), 2065–2070. https://doi.org/10.3382/ps.0652065

Merkx, D. W., Delić, F., Wierenga, P. A., Hennebelle, M., & van Duynhoven, J. P. (2019). 31P NMR assessment of the phosvitin-iron complex in mayonnaise. *Magnetic Resonance in Chemistry, 57*(9), 540–547. https://doi.org/10.1002/mrc.4808

Narayanan, T., Sztucki, M., Van Vaerenbergh, P., Léonardon, J., Gorini, J., Claustre, L., et al. (2018). A multipurpose instrument for time-resolved ultra-small-angle and coherent X-ray scattering. *Journal of Applied Crystallography, 51*(6), 1511–1524. https://doi.org/10.1107/S1600576718012748

Narayanan, T., Sztucki, M., Zinn, T., Kieffer, J., Homs-Puron, A., Gorini, J., … Boesecke, P. (2022). Performance of the time-resolved ultra-small-angle X-ray scattering beamline with the extremely brilliant source. *Journal of Applied Crystallography, 55*(1), 98–111. https://doi.org/10.1107/s1600576721012693

Okur, H. I., Hladílková, J., Rembert, K. B., Cho, Y., Heyda, J., Dzubiella, J., et al. (2017). Beyond the Hofmeister series: Ion-specific effects on proteins and their biological functions. *Journal of Physical Chemistry B, 121*(9), 1997–2014. https://doi.org/10.1021/acs.jpcb.6b10797

Onuma, K. (2005). Effect of phosvitin on the nucleation and growth of calcium phosphates in physiological solutions. *Journal of Physical Chemistry B, 109*(16), 8257–8262. https://doi.org/10.1021/jp044550l

Ottewill, R. H. (1997a). Application of scattering techniques to polymer colloid dispersions. In J. M. Asua (Ed.), *Polymeric dispersions: Principles and applications* (pp. 229–242). Dordrecht: Springer Netherlands. https://doi.org/10.1007/978-94-011-5512-0_16

Ottewill, R. H. (1997b). Scattering techniques-fundamentals. In J. M. Asua (Ed.), *Polymeric dispersions: Principles and applications* (pp. 217–228). Dordrecht: Springer Netherlands. https://doi.org/10.1007/978-94-011-5512-0_15

Philipse, A. P., & Vrij, A. (1988). Determination of static and dynamic interactions between monodisperse, charged silica spheres in an optically matching, organic solvent. *The Journal of Chemical Physics, 88*(10), 6459–6470. https://doi.org/10.1063/1.454432

Skou, S., Gillilan, R. E., & Ando, N. (2014). Synchrotron-based small-angle X-ray scattering of proteins in solution. *Nature Protocols, 9*(7), 1727–1739. https://doi.org/10.1038/nprot.2014.116

Svergun, D. I., & Koch, M. H. (2003). Small-angle scattering studies of biological macromolecules in solution. *Reports on Progress in Physics, 66*(10), 1735–1782. https://doi.org/10.1088/0034-4885/66/10/R05

Taborsky, G. (1963). Interaction between phosvitin and iron and its effect on a rearrangement of phosvitin structure. *Biochemistry, 2*(2), 266–271. https://doi.org/10.1021/bi00902a010

Taborsky, G. (1968). Optical rotatory dispersion of phosvitin at low pH circular Dichroism. *Journal of Biological Chemistry, 243*(22), 6014–6020. https://doi.org/10.1016/S0021-9258(18)94521-7

Taborsky, G. (1983). Phosvitin. *Advances in Inorganic Biochemistry, 5*(7), 235–279. https://doi.org/10.1016/S0021-9258(18)96119-3

Van Gruijthuijsen, K., Obiols-Rabasa, M., Heinen, M., Nägele, G., & Stradner, A. (2013). Sterically stabilized colloids with tunable repulsions. *Langmuir, 29*(36), 11199–11207. https://doi.org/10.1021/la402104q

Yasui, S. C., Pancoska, P., Dukor, R. K., Keiderling, T. A., Renugopalakrishnan, V., Glimcher, M. J., et al. (1990). Conformational transitions in phosvitin with pH variation. *Journal of Biological Chemistry, 265*(7), 3780–3788. https://doi.org/10.1016/S0021-9258(19)39662-0

Yilmaz, B., & Ağagündüz, D. (2020). Bioactivities of hen's egg yolk phosvitin and its functional phosphopeptides in food industry and health. *Journal of Food Science, 85* (10), 2969–2976. https://doi.org/10.1111/1750-3841.15447

Zhang, Y., & Cremer, P. S. (2006). Interactions between macromolecules and ions: The Hofmeister series. *Current Opinion in Chemical Biology, 10*(6), 658–663. https://doi.org/10.1016/j.cbpa.2006.09.020

Zhang, X., Geng, F., Huang, X., & Ma, M. (2016). Calcium binding characteristics and structural changes of phosvitin. *Journal of Inorganic Biochemistry, 159*, 76–81. https://doi.org/10.1016/j.jinorgbio.2016.02.001

Zhang, X., Huang, X., & Ma, M. (2017). Role of phosphorylation of phosvitin in the phase transformation of mineralization. *International Journal of Biological Macromolecules, 101*, 712–718. https://doi.org/10.1016/j.ijbiomac.2017.03.158

Zhang, X., Qiu, N., Geng, F., & Ma, M. (2011). Simply and effectively preparing high-purity phosvitin using polyethylene glycol and anion-exchange chromatography. *Journal of Separation Science, 34*(22), 3295–3301. https://doi.org/10.1002/jssc.201100601

Zhang, F., Skoda, M. W., Jacobs, R. M., Martin, R. A., Martin, C. M., & Schreiber, F. (2007). Protein interactions studied by SAXS: Effect of ionic strength and protein concentration for BSA in aqueous solutions. *Journal of Physical Chemistry B, 111*(1), 251–259. https://doi.org/10.1021/jp0649955

Zhu, Q., Pan, Y., Jia, X., Li, J., Zhang, M., & Yin, L. (2019). Review on the stability mechanism and application of water-in-oil emulsions encapsulating various additives. *Comprehensive Reviews in Food Science and Food Safety, 18*(6), 1660–1675. https://doi.org/10.1111/1541-4337.12482